

1 **Engineering the human Fc-region enables direct cell killing by cancer glycan-targeting**
2 **antibodies without the need for immune effector cells or complement**

3
4 Mireille Vankemmelbeke^{1,2*} Richard S. McIntosh^{1*}, Jia Xin Chua^{1,2}, Thomas Kirk^{1,2}, Ian Daniels²,
5 Marilena Patsalidou¹, Robert Moss¹, Tina Parsons², David Scott³, Gemma Harris⁴, Judith M.
6 Ramage¹, Ian Spendlove¹ and Lindy G. Durrant^{1,2,5}

7
8 **Running title: Fc-engineering direct cytotoxicity in cancer glycan-targeting mAbs**

9
10
11 [1] Academic Department of Clinical Oncology, Division of Cancer and Stem Cells, School of
12 Medicine,

13 University of Nottingham Biodiscovery Institute, University Park, Nottingham, UK

14 [2] Scancell Limited, University of Nottingham Biodiscovery Institute, University Park, Nottingham UK

15 [3] School of Biosciences, University of Nottingham, Sutton Bonington Campus, UK

16 [4] Research Complex at Harwell, Rutherford Appleton Laboratory, Didcot, UK

17
18 * these authors contributed equally to this work

19
20 **Key words:** monoclonal antibody, Fc engineering, cooperative binding, oncosis

21
22 Financial support: This work was supported by MRC-DPFS funding (MR/M015564/1) and Scancell
23 Ltd.

24
25 ⁵Corresponding Author:

26 University of Nottingham Biodiscovery Institute

27 University Park

28 Nottingham NG7 2RD, UK

29 Fax/Phone number: +44 (0)115 8231863

30 E-mail address: lindy.durrant@nottingham.ac.uk

31
32
33 **Disclosure of Potential Conflicts of Interest**

34 L.G. Durrant is a director and CSO of Scancell Ltd. and has shares in Scancell Ltd. MV, JXC, TK, ID

35 and TP are employees of Scancell Ltd.

36

37

38

1 **Abstract**

2 Murine IgG3 glycan-targeting mAb often induces direct cell killing in the absence of immune effector
3 cells or complement via a proinflammatory mechanism resembling oncotic necrosis. This cancer cell
4 killing is due to non-covalent association between Fc regions of neighboring antibodies, resulting in
5 enhanced avidity. Human isotypes do not contain the residues underlying this cooperative binding
6 mode; consequently, the direct cell killing of mouse IgG3 mAb is lost upon chimerization or
7 humanization. Using the Lewis^{a/c/x}-targeting 88mAb, we identified the murine IgG3 residues
8 underlying the direct cell killing and increased avidity via a series of constant region shuffling and
9 subdomain swapping approaches to create improved ('i') chimeric mAb with enhanced tumor killing in
10 vitro and in vivo. Constant region shuffling identified a major CH3 and a minor CH2 contribution,
11 which was further mapped to discontinuous regions among residues 286-306 and 339-378 that, when
12 introduced in 88hIgG1, recapitulated the direct cell killing and avidity of 88mIgG3. Of greater interest
13 was the creation of a sialyl-di-Lewis^a-targeting i129G1 mAb via introduction of these selected
14 residues into 129hIgG1, converting it into a direct cell killing mAb with enhanced avidity and
15 significant in vivo tumor control. The human iG1 mAb, termed Avidimabs, retained effector functions,
16 paving the way for the proinflammatory direct cell killing to promote ADCC and CDC through relief of
17 immunosuppression. Ultimately, Fc engineering of human glycan-targeting IgG1 mAb confers
18 proinflammatory direct cell killing and enhanced avidity, an approach that could be used to improve
19 the avidity of other mAb with therapeutic potential.

20 **Statement of Significance**

21 Fc-engineering enhances avidity and direct cell killing of cancer-targeting anti-glycan antibodies to
22 create superior clinical candidates for cancer immunotherapy.

23

24

1 **Introduction**

2 The cancer glycome is a rich source of targets for monoclonal antibody (mAb) development due to
3 the alterations associated with the transformation process, as well as glycans being key co-accessory
4 molecules for cancer cell survival, proliferation, dissemination and immune evasion (1,2). A number of
5 anti-glycan mAbs are in clinical development, as passive or active immunotherapy or reformatted for
6 chimeric antigen receptor (CAR) T cells (3-5). Additionally, Dinutuximab beta, an anti-GD2 mAb, is
7 currently used for the treatment of neuroblastoma (6).

8 We previously described a panel of cancer glycan targeting mAbs with Lewis^{a/c/x}, Lewis^y (7,8) as well
9 as sialyl-di-Lewis^a reactivity (9). Intriguingly, some of these glycan-binding mAbs exhibited a direct
10 cytotoxic effect on high-density target expressing cancer cells, independent of the presence of
11 complement or immune effector cells. This direct cytotoxic ability has also been observed for other
12 anti-glycan mAbs and typically involves mAb-induced homotypic cellular adhesion, cytoskeletal
13 rearrangement followed by cell swelling, membrane lesions and eventual cellular demise (7,10-13). In
14 most cases the cell death is a form of non-classical apoptosis, potentially involving the generation of
15 reactive oxygen species (ROS), and most closely resembling oncotic necrosis (14,15). Importantly,
16 akin to immunogenic or inflammatory cell death (ICD), the coinciding release of inflammatory
17 mediators - damage associated molecular patterns (DAMPs) - has the potential to recruit innate
18 immune cells to the tumor site that may further increase mAb-mediated effector functions (16). Thus,
19 these anti-glycan mAbs can be important tools to remobilise the full potential of the immune system in
20 an otherwise immunosuppressive environment.

21 The direct killing ability of anti-glycan mAbs is mediated by murine (m) IgG3, an isotype that exhibits
22 non-covalent interactions between adjacent Fc regions, thereby increasing avidity, via prolonging
23 target occupancy; a process termed "intermolecular co-operativity" (17,18). In humans, the IgG2
24 isotype can increase avidity via dimerization involving one or more Cys residues in its hinge region
25 (19). However, this inefficient process, combined with poor ADCC and CDC activity render the hIgG2
26 an unattractive clinical candidate.

27 Our panel of mAbs induce strong *in vitro* and *in vivo* tumor killing in preclinical mouse models (7,8)
28 and thus are candidates for clinical development. Chimerization of the mIgG3 mAbs onto a human
29 IgG1 backbone coincided with a dramatic reduction in direct cytotoxicity, leading us to hypothesize
30 that this was the result of diminished intermolecular cooperativity. Consequently, the rationale for this
31 study was to identify the key residues within mIgG3 that are responsible for non-covalent Fc
32 interactions and transfer them into hIgG1 in order to recapitulate the mIgG3-observed direct
33 cytotoxicity and avidity, thereby creating a chimeric hIgG1 with superior clinical utility.

34 We report here the identification of discontinuous regions within the mIgG3 CH2 and CH3 domains
35 that endow this isotype with direct cytotoxicity and increased avidity. Transfer of these residues into
36 the hIgG1 isotype, creates an improved hIgG1 with increased *in vitro* and *in vivo* anti-tumor activity.

37

38

1 -

2 **Methods**

3 **Materials, cells and antibodies**

4 Colorectal cancer cell lines (COLO205 and HCT15) as well as the murine myeloma NS0 cell line were
5 purchased from ATCC (Virginia, USA). All cell lines were authenticated using short tandem repeat
6 profiling and tested monthly for the presence of Mycoplasma. Human serum albumin (HSA)-APD-
7 sialyl-Lewis^a and HSA-APD-Lewis^a were from IsoSepAB (Sweden). Cell lines were maintained in
8 RPMI medium 1640 (Sigma) supplemented with 10% fetal calf serum, L-glutamine (2mM) and sodium
9 bicarbonate-buffered. Parental murine FG88.2 and FG129 mAbs were generated, as previously
10 described (7);(9)).

11 **Cloning of modified mAb constructs**

12 In order to create chimeric hIgG1 variants of our hybridoma-produced mAbs (FG88.2 and FG129), the
13 heavy chain and light chain variable regions encoding the respective mAbs were introduced into the
14 pDCOrig vector using the restriction enzymes BamHI/BsiWI (light chain locus) or HindIII/AfeI (heavy
15 chain locus) (20). The synthetic heavy chain constant regions (CH), including full mIgG3 constant
16 regions as well as interchanged mIgG3-hIgG1 domains and single residue changes, were designed
17 and ordered from Eurofins MWG (Ebersberg, Germany). Typically, this involved a 1054bp cassette
18 supplied in proprietary Eurofins vectors, stretching from the AfeI restriction site at the VH/CH junction
19 to an XbaI site 3' to the CH stop codon. After maxiprep (Qiagen), 15µg of plasmid DNA was digested
20 with AfeI and XbaI (NEB) and the insert gel-purified (QIAquick, Qiagen) and introduced into AfeI/XbaI
21 digested vector pOrigHiB (20) by ligation (T4 DNA ligase, NEB). Following sequence confirmation,
22 15µg of plasmid DNA was digested with AfeI and AvrII (NEB) and the insert introduced into AfeI/AvrII
23 digested vector pDCOrig by ligation. A cartoon representation of the key Fc-engineered constructs is
24 shown in Supplementary Fig. 5.

25 **HEK293 transfection and mAb purification**

26 mAb constructs were obtained following transient transfections of Expi293F™ cells using the
27 ExpiFectamine™ 293 Transfection kit (Gibco, LifeTechnologies). Briefly, HEK293 cells in suspension
28 (100ml, 2x10⁶/ml) were transfected with 100µg DNA and conditioned medium harvested at day seven
29 post-transfection. mAb-containing supernatant was filtered through 0.22µm bottle top filters (Merck
30 Millipore) and sodium azide added to a final concentration of 0.2% (w/v). mAb was purified on protein
31 G columns (HiTrap ProteinG HP, GE Healthcare) using an AKTA FPLC (GE Healthcare). Columns
32 were washed with PBS/Tris buffer (PBS with 50mM Tris/HCl, pH7.0) before mAb elution with a rapid
33 gradient into 100mM glycine, pH12 (supplemented with 0.05% v/v Tween 20), collecting 2ml fractions.
34 Fractions containing mAb were pooled, neutralized to pH 7.0 (using 1M HCl) and dialyzed against
35 PBS, before concentration determination and storage at -80°C. All transiently expressed mAb
36 constructs were analyzed for cell binding using flow cytometry, as a read-out for correct folding, and
37 compared to the parental 88mIgG3 and 88hIgG1, prior to use in functional assays.

38 **Indirect immunofluorescence and flow cytometry**

39 Cancer cells (1x10⁵) were incubated with primary mAbs (at 33.3nmol/L or titrated) for 1h at 4°C, as
40 previously described (7) followed by 1h incubation at 4°C with anti-mouse or anti-human FITC-

1 labelled secondary antibody, and fixing in 0.4% formaldehyde. Stained samples were analyzed on a
2 MACSQuant 10 flow cytometer and analyzed using FlowJo v10.

3 **Avidity determination**

4 The kinetic parameters of the 88 and 129 mAbs binding to Lewis^a - or sialyl-Lewis^a -APD-HSA were
5 determined by Surface Plasmon Resonance (SPR, Biacore 3000, GE Healthcare). Increasing
6 concentrations (0.3nmol/L-200nmol/L) of mAb were injected across a CM5 chip and data were fitted
7 to a heterogeneous ligand binding model using BIAevaluation 4.1. The chip contained four cells, two
8 of which, HSA-coated (in-line reference cells), the other two were coated with low (30-80 response
9 units (RU)) and high amounts (360-390 RU) of the respective glycan-APD-HSA.

10 ***In vitro* cytotoxicity**

11 Propidium Iodide (PI) uptake and proliferation inhibition were performed to analyze the direct cytotoxic
12 effect of the mAbs. COLO205 or HCT15 cells (5×10^4) were incubated with mAbs for 2h at 37°C
13 followed by the addition of 1µg of PI for 30min. Cells were resuspended in PBS and run on a
14 Beckman Coulter FC-500 or on a MACSQuant 10 flow cytometer and analyzed with WinMDI 2.9 or
15 FlowJo v10 software, respectively. Proliferation inhibition was assessed by using the water-soluble
16 tetrazolium salt WST-8 (CCK8 kit, Sigma-Aldrich) to measure the activity of cellular hydrogenases
17 which is directly proportional to the number of viable cells. Briefly, after overnight plating of cancer
18 cells (1000 cells/90µl/well), constructs were added at different concentrations in a final volume of
19 10µl/well and the plates were incubated at 37°C, (5%CO₂) for 72-96h. WST-8 reagent was then
20 added (10µl/well) and after a further 3h incubation, the plates were read at 450nm (Tecan Infinite F50)
21 and percentage inhibition calculated. EC₅₀ values were determined using nonlinear regression (curve
22 fit) with GraphPad Prism v 8.0 (GraphPad Inc, La Jolla, CA).

23 **Immune effector function determination**

24 ADCC and CDC were performed as described previously (7). ⁵¹Cr-labeled target cells (5×10^3) were
25 co-incubated with 100µL of peripheral blood mononuclear cells (PBMC) from healthy donors (ADCC)
26 or 10% (v/v) autologous serum (CDC) and with mAbs at a range of concentrations; the effector to
27 target ratio was 100:1 (E:T). Spontaneous and maximum release [counts per minute (cpm)] were
28 evaluated by incubating the labelled cells with medium or with 10% (v/v) Triton X-100, respectively.
29 The mean percentage lysis was calculated as follows: mean % lysis = (experimental cpm -
30 spontaneous cpm)/(maximum cpm - spontaneous cpm) × 100.

31 **Scanning electron microscopy**

32 HCT15 or COLO205 cells (1×10^5) were grown on sterile coverslips for 24h prior to mAb (0.2µmol/L)
33 addition for 18h at 37°C. Controls included medium alone and 0.5% (v/v) hydrogen peroxide (H₂O₂)
34 (Sigma). Cells were washed with pre-warmed 0.1 M sodium cacodylate buffer pH7.4 (SDB) and fixed
35 with 12.5% (v/v) glutaraldehyde for 24h. Fixed cells were washed twice with SDB and post-fixed with
36 1% (v/v) osmium tetroxide (pH 7.4) for 45min. After a final wash with H₂O, the cells were dehydrated
37 in increasing concentrations of ethanol and exposed to critical point drying, before sputtering with
38 gold, prior to SEM analysis (JSM-840 SEM, JEOL).

39 **Recombinant human FcRn binding analysis**

1 The ability of the mAbs to bind to recombinant human (rh) FcRn (R&D Systems) was evaluated using
2 direct ELISA at pH6.0 and pH7.0. Briefly, high-binding ELISA plates were coated with 250ng/well
3 rhFcRn followed by blocking with protein-free blocking buffer (Thermo Fisher Scientific). Primary mAb
4 dilutions (in phosphate buffer pH6.0 or pH7.0) were added (1h at room temperature), followed by
5 washing with respective phosphate buffers containing 0.05% (v/v) Tween 20, and detection of bound
6 mAbs with goat F(ab)₂ anti-human IgG(Fab)₂ HRP antibody (Abcam). The anti-hCTLA4 hIgG1 mAb
7 Ipilimumab (clinical grade) was included as a positive control.

8 **Biophysical characterization of the mAbs (size exclusion chromatography with multi-angle 9 light scattering (SEC-MALS) and analytical ultracentrifugation (AUC))**

10 SEC-MALS experiments were performed using a Superose 6 10/300 Increase column (GE
11 Healthcare) on an AktaPure 25 System (GE Healthcare). mAb samples (100µL at 1mg/mL), were
12 loaded and eluted with one column volume (24mL) of buffer, at a flow rate of 0.5mL/min. The eluting
13 protein was monitored using a DAWN HELEOS-II 18-angle light scattering detector (Wyatt
14 Technologies) equipped with a WyattQELS dynamic light scattering module, a U9-M UV/Vis detector
15 (GE Healthcare), and an Optilab T-rEX refractive index monitor (Wyatt Technologies). Data were
16 analyzed by using Astra (Wyatt Technologies) using a refractive index increment value of 0.185mL/g.
17 For AUC characterization, sedimentation velocity scans were recorded for each mAb sample at
18 concentrations of 5.0, 2.5 and 0.5µmol/L. All experiments were performed at 50,000 rpm, using a
19 Beckman Optima analytical ultracentrifuge with an An-50Ti rotor at 20°C. Data were recorded using
20 the absorbance optical detection system at 280nm. The density and viscosity of the buffer was
21 measured experimentally using a DMA 5000M densitometer equipped with a Lovis 200ME viscometer
22 module. The partial specific volume of the antibodies was calculated using SEDFIT from the amino
23 acid sequence. Data were processed using SEDFIT, fitting to the c(s) model. Figures were made
24 using GUSI.

25 **C4d ELISA**

26 Complement activation in normal human serum, in the absence of target, was determined by
27 measuring C4d concentrations, a marker for classical complement pathway activation. mAbs (10%
28 v/v, 100µg/mL) were incubated in 90% normal human serum (three healthy donors) for 1 h at 37°C.
29 C4d concentrations were measured using a commercial ELISA kit (MicroVue C4d EIA kit, Quidel
30 Corporation, San Diego, US) according to the manufacturer's instructions. Heat-aggregated (HA)
31 mAb served as a positive control; the anti-hCTLA4 hIgG1 mAb Ipilimumab (clinical grade) as a
32 reference.

33 ***In vivo* model**

34 The study was conducted and approved by CrownBio UK under a UK Home Office Licence in
35 accordance with NCRI, LASA, and FELAS guidelines. Animal welfare for this study complies with the
36 UK Animals Scientific Procedures Act 1986 (ASPA) in line with Directive 2010/63/EU of the European
37 Parliament and the Council of September 22, 2010 on the protection of animals used for scientific
38 purposes. Subcutaneous tumors of a human colorectal adenocarcinoma model of COLO205 were
39 established in age-matched female BALB/c nude (Charles River, UK) mice via injection of 5×10⁶
40 viable cells in 0.1ml serum free RPMI:Matrigel (1:1) into the left flank of each mouse. Mice (n=10)

1 were randomly allocated to treatment groups based on their mean tumor volume ($\sim 103\text{mm}^3 \pm 13\text{mm}^3$)
2 on study day 6 and dosed intravenously (i.v.), biweekly, with mAbs (0.1mg) or vehicle (PBS, 100 μ l) up
3 until week 5. Body weight and tumor volume were assessed three times weekly and reduction in
4 tumor volume analyzed statistically using two-way ANOVA with Bonferroni's post-test at day 35, when
5 all control animals were still in the study (GraphPad Prism v 7.4, GraphPad Inc, La Jolla, CA).

6 **Statistical analyses**

7 The error bars shown in the figures represent the mean \pm SD. Titration curves for functional assays
8 (direct cell killing, immune effector functions) were analyzed with two-way ANOVA with the construct
9 factor P values graphed. Functional affinity results as well as fixed-concentration functional assays
10 were analyzed with one-way ANOVA with Dunnett's corrections for multiple comparisons. All
11 analyses were performed with GraphPad Prism v 7.4 (GraphPad Inc, La Jolla, CA), with * $P \leq 0.05$, **
12 $P \leq 0.01$, *** $P \leq 0.001$, **** $P \leq 0.0001$.

13

1 Results

2 **m88G3 exhibits avid glycan binding as well as direct cytotoxicity in the absence of** 3 **complement and immune effector cells, both of which are reduced upon chimerization to** 4 **88hlgG1**

5 We have previously shown that the hybridoma-produced mlgG3 mAb FG88.2 exerts a direct
6 cytotoxic effect on high-binding cancer cell lines, such as COLO205 and HCT15, in the absence of
7 complement or effector cells (7). This direct cytotoxicity involved mAb-induced cellular aggregation,
8 proliferation inhibition as well as irregular pore formation through an oncolytic mechanism. We
9 subsequently created a chimeric, HEK293-expressed, hlgG1 mAb, 88hlgG1, for clinical exploitation.
10 88hlgG1 maintained equivalent HCT15 and COLO205 cancer cell binding levels (Fig. 1A), compared
11 to the hybridoma-produced FG88.2, as well as the HEK293-expressed 88mlgG3. The latter mAb was
12 generated to rule out expression system related effects such as differential Fc glycosylation, due to
13 the use of murine hybridoma cells versus HEK293 cells. Surprisingly, 88hlgG1, exhibited significantly
14 reduced direct cytotoxicity on COLO205 and HCT15, across two functional assays, PI uptake and
15 proliferation inhibition, compared to 88mlgG3 (Fig. 1, panels B-D). 88mlgG3 also displayed a modest
16 reduction in direct cytotoxicity compared to the hybridoma-produced FG88.2, suggesting that
17 differential glycosylation of the Fc region by the two expression settings (mouse hybridoma versus
18 HEK293 cells) contributed to the effect. Combined, the results indicated that the direct cell killing
19 could be related to the kinetic binding behaviour of the different isotypes. Consequently, the kinetic
20 binding of our isotype-switched mAbs was analyzed on a Lewis^a-APD-HSA coated chip using SPR (
21 Supplementary Table 1). FG88.2 displayed avid Lewis^a-APD-HSA binding with fast apparent on-rates
22 ($k_{on} \sim 10^4$ 1/smol/L) and very slow off rates ($k_{off} \sim 10^{-6}$ 1/s) on the high-density flow cell. The HEK293-
23 produced 88mlgG3 exhibited an apparent faster on-rate ($k_{on} \sim \times 10^5$ 1/smol/L) and a somewhat faster
24 off-rate ($k_{off} \sim 10^{-4}$ 1/s) compared to FG88.2, that could explain the slightly reduced cytotoxicity
25 compared to FG88.2. In comparison, 88hlgG1 bound its target with an apparent fast on-rate ($k_{on} \sim$
26 10^5 1/smol/L), but in contrast to the mlgG3 isotypes displayed a much faster dissociation phase
27 (apparent $k_{off} \sim 10^{-2}$ 1/s), that is likely to underly its reduced cytotoxic activity upon cancer cell binding.
28 The mAb binding behaviour on the low-density flow cell was largely comparable between the three
29 mAbs, with equilibrium dissociation constants (Kd) of the order of 10^{-8} mol/L for all three isotypes.

31 **Domain analysis of the mlgG3 constant region indicate a major contribution by the mlgG3 CH3** 32 **domain with a minor involvement of the CH2**

33 Collectively, the results outlined above suggested that the high Lewis^a-APD-HSA avidity exhibited
34 by FG88.2 and 88mlgG3, predominantly driven by their slow target dissociation and potentially
35 resulting from the intermolecular cooperativity of the mlgG3 isotype, contributed to their direct
36 cytotoxic effect. We thus set out to engineer a hlgG1 cancer glycan targeting mAb with direct
37 cytotoxic activity, via the transfer of selected mlgG3 constant region residues into 88hlgG1. Firstly,
38 mlgG3 contributing regions were identified through the creation of hybrid 88hlgG1 constructs,
39 containing mlgG3 CH1, CH2 or CH3 domains. Preliminary analyses ascertained that mlgG3 CH1
40 had a negligible contribution to the direct cytotoxicity ability of 88mlgG3, as introducing mlgG3 CH1

1 into 88hlgG1 (1m1) did not lead to a significant increase in cytotoxicity (Fig. 2, Panels A and B).
2 Conversely, introducing hlgG1 CH1 into 88mlgG3 (3h1), equally, did not instigate a significant
3 reduction in killing activity (Fig. 2, Panels A and B). Next, in a gain-of-function approach, the mlgG3
4 CH2 and CH3 domains, separately, were introduced in 88hlgG1. 88hlgG1 containing murine CH3
5 (1m3) exhibited a significant gain in PI uptake on HCT15, as well as a significant increased proliferation
6 inhibition of COLO205 cells, when compared to 88hlgG1 (Fig. 2, Panels C and D). Introducing
7 murine CH2 into 88hlgG1 (1m2) led to small, but not significant, increase in killing activity across both
8 assays (Fig. 2, Panels C and D). As a confirmation of the contributions made by both domains, the
9 reverse strategy was adopted, whereby a loss of cytotoxicity activity was evaluated due to the
10 introduction hlgG1 CH2 or CH3 domains into 88mlgG3. This scenario led to a significant decrease in
11 cytotoxicity for 88mG3 containing hlgG1 CH3 (3h3), corroborating the previous gain-of-function
12 results. Importantly, this strategy also identified a small contribution by the murine CH2, as 88mlgG3
13 containing human CH2 (3h2) exhibited a significant decrease in cytotoxicity activity (Fig. 2, Panels C
14 and D). Next, the kinetic binding behaviour of the hybrid constructs was analyzed. The hybrid
15 construct 1m3 exhibited a modest, but significant increase in avidity (decreased Kd), whilst 3h3,
16 containing human CH3, displayed a significant decrease in avidity (increased Kd, Fig. 2, Panel E), in
17 both cases, mirroring the direct cytotoxicity. Human CH2 in construct 3h2 also led to a modest, but
18 significant drop in avidity. In all cases, the changes in avidity were predominantly driven by changes in
19 the off-rate of the mAbs, with 1m3 showing a significantly decreased off-rate compared to 88hlgG1,
20 whereas 3h3, as well as 3h2, exhibited a significantly increased off-rate compared to 88mlgG3 (Fig.
21 2, panel F). Murine CH2 in construct 1m2 did not lead to increased avidity nor a decreased off-rate,
22 underlying the insignificant cytotoxicity of this construct compared to 88hlgG1 (Fig. 2, panels C and
23 D). Taken together the results indicate that the murine CH3 has a more pronounced contribution to
24 cytotoxicity, as well as kinetic binding, whereas the contribution by murine CH2 is smaller, only
25 observed in a loss-of-function setting.

26

27 **Discontinuous sequences within the CH2-CH3 region of aa 286-397 are essential for killing** 28 **activity and increased avidity**

29 As the cytotoxic effect endowed by the murine CH3 was not complete, and in order to further narrow
30 down the other contributing residues, we designed hybrid 88 mAb constructs where the CH2 and CH3
31 domains were further subdivided into two subdomains (SD) with junction regions containing a 10
32 residue overlap: CH2: SD232-294 and SD286-345 and CH3: SD339-397 and SD390-447. On
33 COLO205, both SD339-397 and SD286-345 afforded a similar significant increase in cytotoxicity,
34 most evident at the lower concentrations, whereas SD232-294, as well as SD390-447, were
35 dispensable for cytotoxicity (Fig. 3, panels A and C). On HCT15 however, the significant contribution
36 by residues within SD339-397 was larger than that of SD286-345 (Fig. 3, panels B and D), suggesting
37 that subtle differences in glyco-antigen density and composition can modulate mAb binding and
38 ensuing cytotoxic activity. Strikingly, 88hlgG1, containing the combined mlgG3 SD286-345 and
39 SD339-397 (SD286-397), recovered virtually all the cytotoxicity of 88mlgG3 on both cell lines and
40 across both assays (Fig. 3, panels A-D), obviating the need for adding additional subdomains. Avidity

1 analysis of the subdomain constructs, compared to 88hlgG1, revealed a striking improvement in
2 avidity for SD286-397, as well as SD339-397, both now matching the 88mIgG3 avidity, with a more
3 modest improvement for SD286-345 (Fig. 3, Panel E). The improved avidity resulted mainly from a
4 dramatically reduced apparent off-rate ($\sim 10^{-6}$ 1/s) for SD286-397 as well as SD339-397, with the
5 SD286-345 off-rate showing a more modest improvement ($\sim 10^{-3}$ 1/s) (Fig. 3, Panel F). These results
6 add further weight to the cytotoxicity observations and support the notion that creating a mAb with a
7 reduced target dissociation rate upholds direct cytotoxicity.

8 Although SD339-397, with 27 mIgG3 residues, recapitulated up to 90% of the desirable attributes of
9 88mIgG3, notably the slow dissociation and enhanced cytotoxicity, it exhibited a significantly reduced
10 CDC activity compared to 88hlgG1 (Fig. 3, Panel G), but it maintained ADCC activity compared to
11 88hlgG1 (Fig. 3, Panel H). The effect on the immune effector functions thus necessitated the use of
12 SD286-397, containing 41 mIgG3 residues for further development. Consequently, additional
13 subdivisions of SD286-345 and SD339-397 were analyzed for cytotoxic activity and avidity in order to
14 further reduce the number of mIgG3 residues. Firstly, within SD339-397, SD339-378, containing 20
15 mIgG3-specific residues, upon introduction in 88hlgG1 led to a significant regain of cytotoxicity to
16 within $\sim 80\%$ to 90% of mIgG3 cytotoxicity across both cytotoxicity assays (Fig. 4, Panels A and B).
17 This region, also instilled a significant increase in avidity, compared to 88hlgG1 (Fig. 4, Panel G), but
18 this improvement was not as pronounced as in the case of SD339-397 (Fig. 3, Panel G). Immune
19 effector functions (ADCC and CDC) of SD339-378 were not significantly different from 88hlgG1 (Fig.
20 4, Panels H and I). Additionally, within SD286-345, the significant reduction in cytotoxicity by SD307-
21 345, compared to SD286-345, implied a further contribution by residues 286-306 (Fig. 4, Panel C).
22 Collectively, the results suggested that a construct containing the combination of residues 286-306
23 and 339-378, totalling 26 mIgG3-specific residues, could potentially fully recapitulate 88mIgG3 direct
24 cytotoxicity and avidity. To test this hypothesis, the cytotoxic activity and avidity of SD286-306+339-
25 378 was evaluated. SD286-306+339-378 exhibited significantly improved direct cytotoxicity,
26 compared to 88 hlgG1, on both cell lines, now matching 88mIgG3 cytotoxicity (Fig. 4, Panels D-F).
27 SPR analysis of SD286-306+339-378 revealed a significantly improved avidity compared to 88hlgG1
28 with a K_d (0.3×10^{-9} nmol/L) now similar to 88mIgG3 (Fig. 4, Panel G). Importantly, neither the CDC
29 activity, nor the ADCC activity of the SD286-306+339-378 construct was significantly different from
30 that of 88hlgG1 (Fig.4, Panels H and I). The combination of improved avidity with direct cytotoxicity,
31 as well as maintained immune effector functions, indicates that our SD286-306+339-378 hybrid hlgG1
32 mimics the desirable attributes of 88mIgG3.

33

1 **Reversal of one *in silico* identified MHCII binding cluster generates the lead candidate,**
2 **improved ‘i’ 88G1, with robust cell killing, increased avidity, pore-forming ability and sound**
3 **immune effector functions**

4 We performed an *in silico* screen of the SD286-306+339-378 sequence, containing 26 mlgG3
5 residues, for MHCII binding epitopes (Immune Epitope Database, IEDB), in order to assess potential
6 immunogenicity. Class II-restricted T helper cells are relevant to the humoral immune response and
7 predicted binding clusters have been shown to be strong indicators of T cell responses (21). Two
8 potential MHCII binding clusters, were identified: cluster 1 (residues 294-315) which would be
9 potentially immunogenic in a wide range of HLA types and cluster 2 (residues 365-393) which would
10 potentially only be weakly immunogenic in HLA-DR*0401 and HLA-DR*01101(Supplementary Fig.1).
11 Reversion of three murine residues, 294 (A to E), 300 (F to Y) and 305 (A to V), within cluster 1, to
12 human residues, produced a human sequence section to which individuals would have been
13 tolerized. Similarly, reversal to human sequence of two residues 351 (I to L) and 371 (N to G), within
14 cluster 2, removed two potential MHCII binding epitopes. Consequently, we created two additional
15 SD286-306+339-378 - based constructs: DI1 and DI2, containing three and two human reverted
16 residues, respectively, and assayed their cytotoxicity and avidity. DI1 maintained significantly
17 improved cytotoxicity compared to 88hlgG1. Additionally, the direct cytotoxicity coincided with a
18 favourable avidity profile, with an apparent off-rate of ($\sim 10^{-4}$ 1/s) and a Kd of 0.5 nmol/L that was
19 similar to 88mlgG3 (Fig. 5, Panel C, Table 1 and Supplementary Fig. 2). In contrast, DI2 showed a
20 small, but consistently decreased activity compared to 88mlgG3 (Fig. 5, Panels A and B) as well as a
21 significantly decreased avidity compared to 88mlgG3 (Fig. 5, Panel C). As this cluster was only
22 potentially weakly immunogenic in two HLA-DR types, these two residues have not been reverted.
23 Instead, we focused on 88DI1, containing 23 mlgG3 residues, now renamed ‘i’ (improved) 88G1, for
24 further analysis of its immune effector functions. 88hlgG1 showed potent ADCC activity on COLO205
25 with sub-nanomolar EC₅₀ (Fig. 5, panel D), in line with the potent immune effector functions of FG88.2
26 (7). Similarly, i88G1 displayed potent ADCC with subnanomolar EC₅₀ (0.35 nmol/L) albeit significantly
27 reduced compared to 88hlgG1 (EC₅₀ 0.13 nmol/L). The CDC activity of i88G1 (EC₅₀ 0.1 nmol/L) was
28 significantly improved compared to 88hlgG1 (3.9 nmol/L) (Fig. 5 Panel E, Table 1).

29 Earlier work on the parental hybridoma-produced FG88.2 had demonstrated its pore-forming ability,
30 which was surmised to underlie its cytotoxicity (7). We thus set out to analyze the pore-forming ability
31 of i88G1 on HCT15, using SEM. Incubation of HCT15 with i88G1 or 88mlgG3, but not 88hlgG1,
32 resulted in monolayer disruption, cell rounding and clustering. At higher magnification, irregular pore
33 formation was evident (Fig. 5 Panel F), mirroring the original data observed for the hybridoma-
34 produced FG88.2 (7).

35 Collectively the results indicate that transfer of selected regions from the mlgG3 constant region into
36 the 88higG1 backbone created a hybrid mAb with direct cell killing ability, increased avidity, pore
37 forming ability as well as robust immune effector functions.

38 **Transfer of the ‘iG1’ sequences into an alternative, non-killing, glycan binding mAb (129**
39 **hlgG1) creates a cancer-targeting mAb with significantly improved avidity and ensuing *in vitro***
40 **and *in vivo* anti-tumor activity**

1 We recently described the generation of a sialyl-di-Lewis^a recognizing mAb (129 mAb) with
2 development potential for cancer immunotherapy (9). The 129 mAb has a more favorable tumor
3 versus normal human tissue distribution compared to the above-described 88 mAb, resulting from
4 wide-ranging tumor tissue binding, combined with very restricted normal tissue reactivity. Neither the
5 hybridoma-produced FG129, a murine IgG1 mAb, nor the chimeric 129hIgG1, exhibited direct
6 cytotoxicity. This led us to test the hypothesis that the introduction of the 23 above-selected mIgG3
7 constant region residues into the Fc region of 129hIgG1 would create an 'i'129G1 with direct
8 cytotoxicity and improved avidity and thus exhibit superior clinical utility.

9 We evaluated the direct cytotoxicity of i129G1 on COLO205, previously shown to be a high-binding
10 cancer cell line for FG129 (9). The i129G1 displayed significantly improved (compared to 129hIgG1),
11 dose-dependent inhibition of proliferation (Fig. 6, Panel A and Table 1), with an EC₅₀ of 45.6 nmol/L,
12 as well as a significantly improved, but more modest, PI uptake (Fig. 6, Panel B). In comparison,
13 negligible direct cytotoxicity was observed on the low to moderate binding ASPC1 or BXP3C
14 (Supplementary Fig. 3). Next, we analyzed the avidity of i129G1 using a sialyl Lewis^a-APD-HSA-
15 coated chip and SPR. The i129G1 mAb exhibited significantly improved avidity compared to
16 129hIgG1 (Fig. 6, panel C, Table 1 and Supplementary Fig. 2), resulting predominantly from an
17 improvement in off-rate by almost two logs ($2.6 \times 10^{-4} \text{ s}^{-1}$ and $5.5 \times 10^{-6} \text{ s}^{-1}$ for 129hIgG1 and i129G1,
18 respectively). On COLO205, i129G1 maintained ADCC activity in the nanomolar range (EC₅₀ 2.4
19 nmol/L), compared to 1.7 nmol/L for 129hIgG1, but the overall percentage lysis was significantly
20 reduced (Fig. 6, panel D, Table 1). The CDC activity of i129G1, however, was significantly increased
21 compared to the parental 129hIgG1, with EC₅₀ of 8.2 nmol/L and 75 nmol/L, respectively (Fig. 6,
22 Panel E, Table 1). The direct cytotoxicity as well as improved avidity of i129G1 led us to analyze its
23 pore-forming ability on COLO205. The incubation of COLO205 with i129G1, caused the formation of
24 large cell clumps with uneven surfaces, as well as the appearance of irregular pore-like structures
25 (Fig. 6, Panel F). Incubation with 129hIgG1, at the same concentration, also led to a degree of cell
26 clumping, but smaller and fewer clumps were observed, without evidence of pore formation.

27 The direct cytotoxicity and improved avidity of i129G1 directed us towards analyzing the *in vivo* anti-
28 tumor activity of i129G1 in comparison with the parental 129hIgG1 in a COLO205 xenograft model.
29 The i129G1 mAb instigated a significant reduction in tumor volume compared to vehicle control (two-
30 way ANOVA, $P < 0.0001$, Fig.6, Panel G and Supplementary Fig. 4) which remained significant when
31 compared to 129hIgG1, thereby corroborating the *in vitro* results. No adverse effects on mean body
32 weight were observed (Fig. 6, Panel H).

33 In order to ascertain that our Fc-engineering approach had not impacted on the biopharmaceutical
34 development potential of the i129G1 mAb, we evaluated its *in vitro* FcRn binding ability, as well as its
35 solution aggregation status using a range of biophysical and biochemical approaches. *In vitro* binding
36 of i129G1 to rhFcRn at pH6.0 and pH7.0 was compared to the parental 129hIgG1 as well as clinically
37 validated Ipilimumab, also a hIgG1. At pH6.0, 129hIgG1 as well as i129G1 display improved binding
38 compared to Ipilimumab. Furthermore, i129G1 exhibited significantly improved rhFcRn binding
39 compared to 129hIgG1 at the highest concentrations tested (Fig. 6, Panel I). Some rhFcRn binding
40 was observed at pH7.0, mainly at the higher concentrations, with the parental 129hIgG1 displaying

1 higher reactivity compared to i129G1. Next, we evaluated the solution-phase characteristics of
2 i129G1 compared to the parental 129hlgG1 using SEC-MALS and AUC. The SEC-MALS profile of
3 129hlgG1 as well as i129G1 were similar, containing a main peak (16-18mL) consistent with an
4 antibody monomer as well as two minor peaks corresponding to higher molecular weight (MW)
5 species (15mL and 8mL (void volume), respectively) (Fig.6, Panel J, i). AUC profiles of both mAbs
6 across the three concentrations tested, revealed a slight increase in the number of higher MW
7 species for i129v1, the main mAb monomer peak being $80.6\% \pm 2.6\%$ and $67.6\% \pm 2.3\%$ of all
8 species detected in the sample for 129hlgG1 and i129v1, respectively (Fig.6, Panel J, ii). The latter
9 analysis prompted us to investigate whether the small increase in higher molecular weight species in
10 the i129v1 sample would lead to complement activation in normal human serum in the absence of
11 antigen engagement. A commercial C4d detection kit (indicating classical complement pathway
12 activation) was used and the analysis performed with serum from three healthy donors. Whereas
13 heat-aggregated (HA) mAb instigated a significant increase in C4d levels upon incubation with human
14 serum, neither i129G1, nor 129hlgG1 caused significant elevation of C4d above the background
15 (Fig.6, Panel J, iii).
16

1 Discussion

2 Whereas unmodified cancer glycan-targeting mAbs often exhibit anti-tumor activity in preclinical
3 animal models, they perform disappointingly in the clinic (3,22-24). One possible explanation is that
4 mIgG3 anti-glycan mAbs exhibited direct cytotoxic activity, which was significantly reduced when
5 chimerized or humanized to hIgG1 (10-13). Similarly, the Lewis^{a/c/x} FG88.2 used in this study, a
6 mIgG3 isotype, exhibited high avidity as well as direct cytotoxicity upon binding to high target-
7 expressing cancer cells (7), both of which were significantly reduced on chimerization to hIgG1.

8 It is perhaps not surprising that the direct cytotoxicity of cancer glycan-targeting mIgG3 mAbs was
9 reduced upon chimerization to a hIgG1 isotype, in view of the well-documented effect of mAb
10 constant regions on variable region affinity and specificity (25-30). However, constant region-driven
11 allosteric effects (intramolecular) tend to be mAb and target specific (27). Greenspan *et al.* on the
12 other hand, surmised that mIgG3 intermolecular cooperativity - enhanced binding through stabilization
13 of non-covalent interactions between neighbouring bound mAbs - brought about increased avidity for
14 multivalent antigen and ensuing isotype restriction (18,31,32). Improved avidity, resulting mainly from
15 slower kinetic off-rates by mIgG3 mAbs, compared to other isotypes, has also been observed by
16 others and resulted in more effective binding at high epitope density (33-37). A number of
17 multimerization strategies with human isotype mAbs have attempted to recreate this increased avidity
18 for cancer antigens, but these were inefficient or unstable (38-40). Additionally, a plethora of Fc
19 engineering strategies, mostly to impact on mAb effector functions (ADCC and CDC), through
20 modifying FcγR or C1q binding, as well as mAb half-life, via FcRn engagement, have been described
21 (41,42). Interestingly, crystal packing-induced mAb oligomerization through Fc:Fc interactions in a
22 number of human mAb isotypes (43-46) formed the basis of a recently described hexameric mAb
23 platform for improved complement activation (47-49). The aforementioned HexaBody technology
24 centred on two positions (E345 and E430) the mutation of which significantly enhanced CDC activity,
25 without impacting on other key pharmacokinetic and biopharmaceutical properties. Our approach on
26 the other hand, focused on improving direct cell killing of glycan-targeting mAbs through engineering
27 increased avidity, mirroring a common ability observed for the murine IgG3 isotype. Advantageously,
28 there is no requirement for complement or immune effector cells and as such our strategy may be
29 less susceptible to immune-suppression in the tumor microenvironment.

30 In the current study we describe the creation of hIgG1 anti-glycan mAbs with increased avidity and
31 direct cytotoxic activity through the transfer of selected mIgG3 constant region residues. Candidate
32 residues were identified through screens based on increased direct cytotoxicity and avidity, when
33 introduced into hIgG1 (gain-of-function), and/or decreased direct cytotoxicity and avidity when
34 replaced by the respective hIgG1 residues in mIgG3 (loss-of-function), using the Lewis^{a/c/x} FG88.2.

35 Differences in segmental flexibility between the two mAbs due to the changed CH1 and hinge
36 regions as well as a direct contribution by murine IgG3 CH1 were ruled out, as the introduction of
37 murine IgG3 CH1 into 88hIgG1 did not increase direct cytotoxicity. Neither did the introduction of
38 hIgG1 CH1 into 88mIgG3 decrease direct cytotoxicity. The murine IgG3 hinge region has somewhat
39 greater flexibility, compared to other murine isotypes (50), but an involvement of the hinge region, in

1 isolation, is unlikely to be solely responsible for the observed direct cytotoxicity and improved avidity,
2 as was recently shown for an erythrocyte glycan binding mIgG3 mAb (36).

3 Focusing on the mIgG3 Fc region, a major contribution by CH3 was identified, with effects evident in
4 improved cytotoxicity as well as avidity, the latter mainly the result of a decreased dissociation rate. A
5 minor contribution by CH2 was only evident when screened via the loss-of-function approach,
6 suggesting a less dominant effect. Similarly, in this setting, the decreased avidity coincided with an
7 increased dissociation rate. An analogous analysis identified a contribution by both CH2 and CH3
8 domain in protective mIgG3 mAbs directed at the capsular antigen of *Bacillus anthracis* (37). More
9 recently, Klaus et al. performed a comprehensive evaluation of mIgG3 constant region contributions
10 to blood glycan avidity (36). Although they attributed a stronger role for the mIgG3 CH2 domain, an
11 effect of CH3 domain was also noted and led to the overall conclusion that the increased avidity of the
12 mIgG3 isotype was likely the result of additive effects through CH domain interplay.

13 Further dissection of the combined CH2CH3 region through subdomain analysis revealed full regain
14 of 88mIgG3 direct cytotoxicity by a section, encompassing the CH2CH3 junction ('elbow'), residues
15 286-397. This stretch of residues contained the combined effects of the dominant CH3 element
16 (residues 339-397) as well as the subdominant CH2 contribution (residues 286-345). Although the
17 CH3 element (339-397) in isolation led to an improved avidity, as well as cytotoxicity, unfortunately, it
18 coincided with significantly reduced CDC compared to 88hIgG1. This is likely an indirect,
19 conformational, effect on C1q binding, as, although close to known C1q interacting residues, none of
20 the 339-397 residues are directly-interacting (47,51). It however necessitated the analysis of residues
21 in the region of 286-397 for further refinement of contributing elements.

22 The introduction into 88hIgG1 of a discontinuous section comprising residues 286-306 and 339-378,
23 recapitulated 88mIgG3 cytotoxicity and avidity, whilst maintaining immune effector functions (ADCC
24 and CDC). The likely explanation for the greater than anticipated number of mIgG3 residues required
25 for increased avidity through intermolecular cooperativity is the combined effect of directly interacting
26 as well as conformational residues, the latter potentially creating a permissive framework. A role for
27 charge distribution patterns, notably in CH2, can also not be ruled out, as it has been shown to
28 enhance mIgG3 binding to negatively charged multivalent antigen and is distinct from hIgG1 (36,37).

29 The introduction of 26 mIgG3 in hIgG1 may create MHCII binding epitopes that have the potential to
30 drive HAMA responses in patients. IEDB analysis of the 26 mIgG3 residue-containing hybrid
31 88hIgG1, revealed two clusters (residues 294-315 and 365-378), one containing several potentially
32 high-scoring epitopes. Residues in cluster 1, at positions 294, 300 and 305, were reverted to human
33 sequence with maintained avidity and direct cytotoxicity. On the other hand, reverting residues at
34 positions 351 and 371 (cluster 2, with weaker binding scores) led to a small but significant decreased
35 cytotoxicity, hence were maintained in the final construct. Importantly, this superior 88hIgG1 hybrid
36 mAb, with mIgG3-matching direct cytotoxicity and avidity, induced cellular aggregation, pore formation
37 and cell lysis on high-binding HCT15, suggesting a similar cell killing mechanism compared to the
38 parental FG88.2 (7). The pore formation and eventual cell lysis share similar cellular disintegration

1 features with necroptosis, but cannot be distinguished from necrosis or secondary necrosis (52). The
2 eventual outcome from the released DAMPs - constitutive or induced as a result of activated stress
3 pathways – during this inflammatory cell death depends on the cellular environment as well as the
4 underlying signalling cascades, but collectively have the potential to create an inflammatory
5 environment that may further enhance immune effector functions and/or instigate an adaptive immune
6 response through cross-presentation of released tumor antigens (16,53). Advantageously, i88G1
7 maintained immune effector functions with CDC activity being significantly improved, and ADCC
8 activity being somewhat reduced, compared to 88hlgG1. As the Fc residues involved in
9 Fcγ3R1/R1 binding are predominantly located in the lower hinge and adjacent top of CH2
10 region, it is unlikely that our introduced changes have a direct effect on this interaction, but we cannot
11 rule out an indirect effect (54).

12 Further validation of our approach, came from the introduction of the selected 23 mlgG3 residues
13 into the sialyl-di-Lewis^a targeting 129hlgG1, that has a more favorable normal tissue distribution whilst
14 targeting a wide range of tumor tissues on tumor microarray analyses, notably binding over 70% of
15 pancreatic, and over 30% of gastric and colorectal tumor tissues, as well as over 20% of ovarian and
16 non-small cell lung cancer tumor tissues (9). Interestingly, the hybridoma-produced parental FG129 is
17 a mlgG1, that lacks direct cytotoxic ability. Thus, the creation of i129G1 with significantly improved
18 avidity, through a slower dissociation rate, compared to 129hlgG1, coinciding with nanomolar direct
19 cell killing ability on COLO205 suggests that our approach may have broader applicability, as well as
20 being relevant for immunomodulatory mAbs that rely on avidity effects (41). The direct cell killing
21 exerted by i129G1 manifested itself in a similar manner as for i88G1: mAb-induced cellular
22 aggregation followed by pore formation and eventual cell lysis. The introduction of the mlgG3
23 residues into i129G1 mAb had a mixed effect on effector functions: whilst overall ADCC-induced cell
24 lysis was significantly reduced, i129G1 maintained nanomolar EC₅₀. The CDC activity of i129G1 on
25 the other hand was significantly increased. This mirrored the results obtained with i88G1, albeit with
26 a stronger reduction in ADCC for i129G1, suggesting that the nature of the glycotarget also affects
27 ADCC potency: whereas the FG88.2 targets glycoproteins as well as glycolipids, the FG129 only
28 targets glycoproteins. Our improved mAb construct, i129G1 exhibited significant tumor volume
29 reduction in a COLO205 xenograft model in nude mice. Remarkably, i129G1 displayed effective
30 tumor control that was significantly better than 129hlgG1, the latter exhibiting no significant tumor
31 reduction, further emphasizing the value of direct cytotoxic ability.

32 Additionally, it was important to ascertain that our Fc-engineering had not impacted on the solution
33 self-association of i129G1. Although the biophysical analysis suggested a small increase in the
34 proportion of higher MW species in the i129G1 sample, more apparent from AUC than SEC-MALS,
35 this did not result in a significantly increased C4d generation upon incubation with healthy human
36 donor serum. We did not observe a reduction in rhFcRn by i129G1 binding, suggesting that the
37 pharmacokinetic aspects equally had not been compromised by our Fc-engineering.

38 The creation of improved cancer glycan targeting mAbs, with enhanced avidity as well as direct
39 cytotoxicity, through establishing intermolecular cooperativity binding, may lead to superior clinical

1 utility. Additionally, it is plausible that mAb multimerization upon glycan target engagement through
2 alternative strategies may equally lead to increased avidity and ensuing direct cytotoxicity. Our
3 approach may also have value for mAbs targeting cancer-associated proteins, where longer target
4 residence time may lead to more profound biological effects, but this remains to be validated.
5 Importantly, reinstating the unusual, proinflammatory cell killing mode observed for many glycan-
6 targeting mIgG3 mAbs, into the hIgG1 framework, opens the door to combination immunotherapy.

7 **Acknowledgments**

8 We are grateful for expert technical assistance with EM work (Denise Mclean, Advanced Microscopy
9 Unit, School of Life Sciences) and for Biacore access (Prof Stephanie Allen, School of Pharmacy),
10 University of Nottingham. This work was supported by a Developmental Pathway Funding Scheme
11 grant from MRC (UK).

1 grant from MRC-UK,

2 **References**

3

- 4 1. Dalziel M, Crispin M, Scanlan CN, Zitzmann N, Dwek RA. Emerging principles for the therapeutic
5 exploitation of glycosylation. *Science* **2014**;343:1235681
- 6 2. Rodriguez E, Schettters STT, van Kooyk Y. The tumour glyco-code as a novel immune checkpoint
7 for immunotherapy. *Nat Rev Immunol* **2018**;18:204-11
- 8 3. Burris HA, 3rd, Rosen LS, Rocha-Lima CM, Marshall J, Jones S, Cohen RB, *et al.* Phase 1
9 experience with an anti-glycotope monoclonal antibody, RAV12, in recurrent adenocarcinoma.
10 *Clinical cancer research : an official journal of the American Association for Cancer Research*
11 **2010**;16:1673-81
- 12 4. Labrada M, Dorvignit D, Hevia G, Rodriguez-Zhurbenko N, Hernandez AM, Vazquez AM, *et al.*
13 GM3(Neu5Gc) ganglioside: an evolution fixed neoantigen for cancer immunotherapy. *Semin Oncol*
14 **2018**;45:41-51
- 15 5. Hege KM, Bergsland EK, Fisher GA, Nemunaitis JJ, Warren RS, McArthur JG, *et al.* Safety, tumor
16 trafficking and immunogenicity of chimeric antigen receptor (CAR)-T cells specific for TAG-72 in
17 colorectal cancer. *J Immunother Cancer* **2017**;5:22
- 18 6. Ladenstein R, Potschger U, Valteau-Couanet D, Luksch R, Castel V, Yaniv I, *et al.* Interleukin 2
19 with anti-GD2 antibody ch14.18/CHO (dinutuximab beta) in patients with high-risk neuroblastoma
20 (HR-NBL1/SIOPEN): a multicentre, randomised, phase 3 trial. *Lancet Oncol* **2018**;19:1617-29
- 21 7. Chua JX, Vankemmelbeke M, McIntosh RS, Clarke PA, Moss R, Parsons T, *et al.* Monoclonal
22 Antibodies Targeting LecLex-Related Glycans with Potent Antitumor Activity. *Clinical cancer*
23 *research : an official journal of the American Association for Cancer Research* **2015**
- 24 8. Noble P, Spendlove I, Harding S, Parsons T, Durrant LG. Therapeutic targeting of Lewis(y) and
25 Tivadar ST, McIntosh RS, Chua JX, Moss R, Parsons T, Zaitoun AM, *et al.* Monoclonal Antibody
27 Targeting Sialyl-di-Lewis(a)-Containing Internalizing and Noninternalizing Glycoproteins with
28 Cancer Immunotherapy Development Potential. *Mol Cancer Ther* **2020**;19:790-801
- 29 10.Loo D, Pryer N, Young P, Liang T, Coberly S, King KL, *et al.* The glycotope-specific RAV12
30 monoclonal antibody induces oncosis in vitro and has antitumor activity against gastrointestinal
31 adenocarcinoma tumor xenografts in vivo. *Mol Cancer Ther* **2007**;6:856-65
- 32 11.Faraj S, Bahri M, Fougeray S, El Roz A, Fleurence J, Veziere J, *et al.* Neuroblastoma
33 chemotherapy can be augmented by immunotargeting O-acetyl-GD2 tumor-associated
34 ganglioside. *Oncoimmunology* **2017**;7:e1373232
- 35 12.Roque-Navarro L, Chakrabandhu K, de Leon J, Rodriguez S, Toledo C, Carr A, *et al.* Anti-
36 ganglioside antibody-induced tumor cell death by loss of membrane integrity. *Mol Cancer Ther*
37 **2008**;7:2033-41
- 38 13.Welt S, Carswell EA, Vogel CW, Oettgen HF, Old LJ. Immune and nonimmune effector functions
39 of IgG3 mouse monoclonal antibody R24 detecting the disialoganglioside GD3 on the surface of
40 melanoma cells. *Clin Immunol Immunopathol* **1987**;45:214-29
- 41 14.Zheng JY, Tan HL, Matsudaira PT, Choo A. Excess reactive oxygen species production mediates
42 monoclonal antibody-induced human embryonic stem cell death via oncosis. *Cell Death Differ*
43 **2017**;24:546-58
- 44 15.Hernandez AM, Rodriguez N, Gonzalez JE, Reyes E, Rondon T, Grinan T, *et al.* Anti-NeuGcGM3
45 antibodies, actively elicited by idiotypic vaccination in nonsmall cell lung cancer patients, induce
46 tumor cell death by an oncosis-like mechanism. *J Immunol* **2011**;186:3735-44
- 47 16.Galluzzi L, Buque A, Kepp O, Zitvogel L, Kroemer G. Immunogenic cell death in cancer and
48 infectious disease. *Nat Rev Immunol* **2017**;17:97-111
- 49 17.Cooper LJ, Schimenti JC, Glass DD, Greenspan NS. H chain C domains influence the strength of
50 binding of IgG for streptococcal group A carbohydrate. *J Immunol* **1991**;146:2659-63
- 51 18.Greenspan NS, Dacek DA, Cooper LJ. Cooperative binding of two antibodies to independent
52 antigens by an Fc-dependent mechanism. *FASEB J* **1989**;3:2203-7
- 53 19.Yoo EM, Wims LA, Chan LA, Morrison SL. Human IgG2 can form covalent dimers. *J Immunol*
54 **2003**;170:3134-8
- 55 20.Metheringham RL, Pudney VA, Gunn B, Towey M, Spendlove I, Durrant LG. Antibodies designed
56 as effective cancer vaccines. *MAbs* **2009**;1:71-85

- 1 21. Jawa V, Cousens LP, Awwad M, Wakshull E, Kropshofer H, De Groot AS. T-cell dependent
2 immunogenicity of protein therapeutics: Preclinical assessment and mitigation. *Clin Immunol*
3 **2013**;149:534-55
- 4 22. Mita MM, Nemunaitis J, Grilley-Olson J, El-Rayes B, Bekaii-Saab T, Harvey RD, *et al.* Phase 1
5 Study of CEP-37250/KHK2804, a Tumor-specific Anti-glycoconjugate Monoclonal Antibody, in
6 Patients with Advanced Solid Tumors. *Target Oncol* **2016**;11:807-14
- 7 23. Horta ZP, Goldberg JL, Sondel PM. Anti-GD2 mAbs and next-generation mAb-based agents for
8 cancer therapy. *Immunotherapy* **2016**;8:1097-117
- 9 24. Forero A, Shah J, Carlisle R, Triozzi PL, LoBuglio AF, Wang WQ, *et al.* A phase I study of an anti-
10 GD3 monoclonal antibody, KW-2871, in patients with metastatic melanoma. *Cancer Biother*
11 *Radiopharm* **2006**;21:561-8
- 12 25. Janda A, Bowen A, Greenspan NS, Casadevall A. Ig Constant Region Effects on Variable Region
13 Structure and Function. *Front Microbiol* **2016**;7:22
- 14 26. Casadevall A, Janda A. Immunoglobulin isotype influences affinity and specificity. *Proc Natl Acad*
15 *Sci U S A* **2012**;109:12272-3
- 16 27. Yang D, Kroe-Barrett R, Singh S, Roberts CJ, Laue TM. IgG cooperativity - Is there allostery?
17 Implications for antibody functions and therapeutic antibody development. *MAbs* **2017**;9:1231-52
- 18 28. Cooper LJ, Shikhman AR, Glass DD, Kangisser D, Cunningham MW, Greenspan NS. Role of
19 heavy chain constant domains in antibody-antigen interaction. Apparent specificity differences
20 among streptococcal IgG antibodies expressing identical variable domains. *J Immunol*
21 **1993**;150:2231-42
- 22 29. Torres M, Casadevall A. The immunoglobulin constant region contributes to affinity and specificity.
23 *Trends Immunol* **2008**;29:91-7
- 24 30. McCloskey N, Turner MW, Steffner P, Owens R, Goldblatt D. Human constant regions influence
25 the antibody binding characteristics of mouse-human chimeric IgG subclasses. *Immunology*
26 **1996**;88:169-73
- 27 31. Greenspan NS, Cooper LJ. Cooperative binding by mouse IgG3 antibodies: implications for
28 functional affinity, effector function, and isotype restriction. *Springer Semin Immunopathol*
29 **1993**;15:275-91
- 30 32. Greenspan NS, Cooper LJ. Intermolecular cooperativity: a clue to why mice have IgG3? *Immunol*
31 *Today* **1992**;13:164-8
- 32 33. Cooper LJ, Robertson D, Granzow R, Greenspan NS. Variable domain-identical antibodies exhibit
33 IgG subclass-related differences in affinity and kinetic constants as determined by surface
34 plasmon resonance. *Mol Immunol* **1994**;31:577-84
- 35 34. Yelton D. An IgG3 antitumor antibody showing cooperative binding mediated by the constant
36 region. 1992 1992.
- 37 35. Loibner H, Janzek E, Plot R. Fc-dependent binding self-cooperativity of a murine IgG3 antitumor
38 mAb as demonstrated by biospecific interaction analysis - comparison with murine switch variants
39 and mouse/human chimeras. 1992 1992.
- 40 36. Klaus T, Bereta J. CH2 Domain of Mouse IgG3 Governs Antibody Oligomerization, Increases
41 Functional Affinity to Multivalent Antigens and Enhances Hemagglutination. *Front Immunol*
42 **2018**;9:1096
- 43 37. Hovenden M, Hubbard MA, Aucoin DP, Thorkildson P, Reed DE, Welch WH, *et al.* IgG subclass
44 and heavy chain domains contribute to binding and protection by mAbs to the poly gamma-D-
45 glutamic acid capsular antigen of *Bacillus anthracis*. *PLoS Pathog* **2013**;9:e1003306
- 46 38. Wolff EA, Schreiber GJ, Cosand WL, Raff HV. Monoclonal antibody homodimers: enhanced
47 antitumor activity in nude mice. *Cancer Res* **1993**;53:2560-5
- 48 39. Hu J, Liu X, Hughes D, Esteva FJ, Liu B, Chandra J, *et al.* Herceptin conjugates linked by EDC
49 boost direct tumor cell death via programmed tumor cell necrosis. *PLoS One* **2011**;6:e23270
- 50 40. Caron PC, Laird W, Co MS, Avdalovic NM, Queen C, Scheinberg DA. Engineered humanized
51 dimeric forms of IgG are more effective antibodies. *J Exp Med* **1992**;176:1191-5
- 52 41. Wang X, Mathieu M, Brezski RJ. IgG Fc engineering to modulate antibody effector functions.
53 *Protein Cell* **2018**;9:63-73
- 54 42. Carter PJ. Potent antibody therapeutics by design. *Nat Rev Immunol* **2006**;6:343-57
- 55 43. Saphire EO, Parren PW, Pantophlet R, Zwick MB, Morris GM, Rudd PM, *et al.* Crystal structure of
56 a neutralizing human IGG against HIV-1: a template for vaccine design. *Science* **2001**;293:1155-9
- 57 44. Davies AM, Rispens T, Ooijevaar-de Heer P, Gould HJ, Jefferis R, Aalberse RC, *et al.* Structural
58 determinants of unique properties of human IgG4-Fc. *J Mol Biol* **2014**;426:630-44
- 59 45. Davies AM, Jefferis R, Sutton BJ. Crystal structure of deglycosylated human IgG4-Fc. *Mol*
60 *Immunol* **2014**;62:46-53

- 1 46. Wu Y, West AP, Jr., Kim HJ, Thornton ME, Ward AB, Bjorkman PJ. Structural basis for enhanced
2 HIV-1 neutralization by a dimeric immunoglobulin G form of the glycan-recognizing antibody 2G12.
3 Cell Rep **2013**;5:1443-55
- 4 47. Ugurlar D, Howes SC, de Kreuk BJ, Koning RI, de Jong RN, Beurskens FJ, *et al.* Structures of C1-
5 IgG1 provide insights into how danger pattern recognition activates complement. Science
6 **2018**;359:794-7
- 7 48. de Jong RN, Beurskens FJ, Verploegen S, Strumane K, van Kampen MD, Voorhorst M, *et al.* A
8 Novel Platform for the Potentiation of Therapeutic Antibodies Based on Antigen-Dependent
9 Formation of IgG Hexamers at the Cell Surface. PLoS Biol **2016**;14:e1002344
- 10 49. Diebolder CA, Beurskens FJ, de Jong RN, Koning RI, Strumane K, Lindorfer MA, *et al.*
11 Complement is activated by IgG hexamers assembled at the cell surface. Science **2014**;343:1260-
12 3
- 13 50. Dangl JL, Wensel TG, Morrison SL, Stryer L, Herzenberg LA, Oi VT. Segmental flexibility and
14 complement fixation of genetically engineered chimeric human, rabbit and mouse antibodies.
15 EMBO J **1988**;7:1989-94
- 16 51. Duncan AR, Winter G. The binding site for C1q on IgG. Nature **1988**;332:738-40
- 17 52. Vanden Berghe T, Vanlangenakker N, Parthoens E, Deckers W, Devos M, Festjens N, *et al.*
18 Necroptosis, necrosis and secondary necrosis converge on similar cellular disintegration features.
19 Cell Death Differ **2010**;17:922-30
- 20 53. Yatim N, Cullen S, Albert ML. Dying cells actively regulate adaptive immune responses. Nat Rev
21 Immunol **2017**;17:262-75
- 22 54. Wines BD, Powell MS, Parren PW, Barnes N, Hogarth PM. The IgG Fc contains distinct Fc
23 receptor (FcR) binding sites: the leukocyte receptors Fc gamma RI and Fc gamma RIIa bind to a
24 region in the Fc distinct from that recognized by neonatal FcR and protein A. J Immunol
25 **2000**;164:5313-8
- 26

1
2
3
4
5
6

Table 1. Overview of the functional characteristics of the improved constructs

Biological activity characteristics					
mAb	avidity ^b Kd (nmol/L)	direct cytotoxicity ^a EC ₅₀ (nmol/L)	ADCC EC ₅₀ (nmol/L)	CDC EC ₅₀ (nmol/L)	Pore forming ability
88mIgG3	0.3	26.7	ND	ND	+++
88hIgG1	48.3	N/A	0.13	3.9	-
i88G1	0.5	29.4	0.35	0.1	++
129hIgG1	2.5	N/A	1.7	75.3	-
i129G1	0.005	45.6	2.4	8.2	++

7 ^adeduced from proliferation inhibition on COLO205
8 N/A: not appropriate, ND: not determined
9 ^bsensorgrams underlying the avidity determination are shown in Supplementary Fig. 2
10
11

1 **Figure Legends**

2 **Figure 1. Maintenance of cancer cell binding, but significantly decreased direct cytotoxicity of**
3 **88hlgG1 compared to 88mlgG3 and parental hybridoma mAb, FG88.2** - Comparable HCT15 and
4 COLO205 cell binding by 88hlgG1, 88mlgG3 and FG88.2 (hybridoma mAb)(Panel A). Significantly
5 reduced direct cytotoxicity (PI uptake) on HCT15 by 88hlgG1 compared to 88mlgG3 and FG88.2
6 (Panel B). Significantly reduced proliferation inhibition by 88hlgG1 compared to 88mlgG3 and FG88.2
7 on COLO205 (Panel C) and HCT15 (Panel D). Significance (88hlgG1 compared to 88mlgG3)
8 deduced from two-way ANOVA.

9 **Figure 2. mlgG3 CH3 and to a lesser extent CH2 contribute to the direct cytotoxicity and**
10 **improved avidity** - Constant domain shuffling suggests no significant contribution by CH1 to direct
11 cytotoxicity (PI uptake, HCT15, Panel A; proliferation inhibition on COLO205, panel B). In contrast,
12 CH3 (1m3 and 3h3) contributes significantly to direct cytotoxicity, with a minor contribution by mCH2
13 only evident in a loss-of-function approach (3h2) (PI uptake, HCT15, Panel C; proliferation inhibition,
14 COLO205, panel D). Significance versus the respective parental constructs was deduced from two-
15 way ANOVA. Significantly increased avidity and decreased off-rate by 1m3; with significantly
16 decreased avidity and increased off-rate by 3h2 and more pronounced by 3h3, confirming the major
17 CH3 and minor CH2 contributions (Panel E, F). Significance deduced using one-way ANOVA, with
18 Dunnett's corrections for multiple comparisons.

19 **Figure 3. SD286-397 encompassing the CH2:CH3 junction underlies mlgG3 direct cytotoxicity**
20 **and improved avidity** - Subdomain divisions of CH2CH3 identified two regions that did not
21 contribute: SD232-294 and SD390-447, as well as two regions that significantly contributed to direct
22 cytotoxicity and avidity: SD286-345 (CH2) as well as SD339-397 (CH3). Significantly increased PI
23 uptake by both constructs and the combination (SD286-397) compared to 88hlgG1 on COLO205
24 (Panel A) and HCT15 (Panel B). Significantly increased proliferation inhibition by both constructs and
25 the combination compared to 88hlgG1 on COLO205 (Panel C) and HCT15 (Panel D). Significance
26 (Panels A – D) was deduced from two-way ANOVA. Significantly increased avidity (SPR), resulting
27 mainly from reduced off-rates by SD286-345 and SD339-397, as well as the combination (SD286-
28 397) (Panels E and F, respectively). Significantly reduced CDC activity (HCT15) by SD339-397
29 compared to 88hlgG1 (Panel G); maintenance of ADCC activity (COLO205) by the aforementioned
30 constructs (Panel H). Significance versus respective parental constructs (Panels E-H) was deduced
31 from one-way ANOVA, with Dunnett's corrections for multiple comparisons.

32 **Figure 4. Discontinuous regions consisting of 286-306 combined with 339-378 impart direct**
33 **cytotoxicity and enhanced avidity, whilst maintaining immune effector functions** - Significantly
34 increased PI uptake (Panel A) and proliferation inhibition (Panel B) by SD339-378 compared to
35 88hlgG1 on HCT15. Significantly reduced proliferation inhibition by SD307-345 compared to SD286-
36 345, suggesting a contribution by SD286-306 (Panel C). Significantly increased proliferation inhibition
37 by the combination of SD286-306+339-378 compared to 88hlgG1 on HCT15 (Panel D) and COLO205
38 (Panel E), as well as PI uptake on COLO205 (Panel F). Significantly increased avidity (SPR) by
39 SD339-378 as well as SD286-306+339-378 compared to 88hlgG1 (Panel G). Maintenance of CDC
40 activity on HCT15 (Panel H) and ADCC on COLO205 (Panel I) by SD339-378 as well as SD286-
41 306+339-378 compared to 88hlgG1. Significance versus respective parental constructs was deduced
42 from two-way ANOVA (direct cytotoxicity) or one-way ANOVA with Dunnett's corrections for multiple
43 comparisons(avidity, and effector functions).

44 **Figure 5. i88G1 with direct cytotoxicity and enhanced avidity, whilst maintaining immune**
45 **effector functions, exhibits pore forming ability** - Reversion to human sequence of three residues
46 in IEDB-predicted MHCII binding cluster 1 (Supplementary Fig.1) created the lead candidate i88G1
47 (DI1). Significantly increased proliferation inhibition on HCT15 (Panel A) and COLO205 (Panel B) by
48 i88G1 compared to 88hlgG1, now matching 88mlgG3 activity. Significance deduced from two-way
49 ANOVA. DI2 displayed a consistent reduction in cytotoxicity compared to DI1 (Panel A and B).
50 Significantly increased avidity (SPR) by i88G1 compared to 88hlgG1, significantly decreased avidity
51 by DI2 compared to 88mlgG3 (Panel C), one-way ANOVA with Dunnett's corrections for multiple
52 comparisons. Significantly reduced, yet remaining subnanomolar, ADCC (COLO205, Panel D) as
53 well as, significantly improved CDC (HCT15, Panel E) activity by i88G1 compared to 88hlgG1 (two-

1 way ANOVA). Evidence of cellular detachment, aggregation and pore formation (white arrows point to
2 irregular pores) by i88G1 on HCT15 (Panel F).

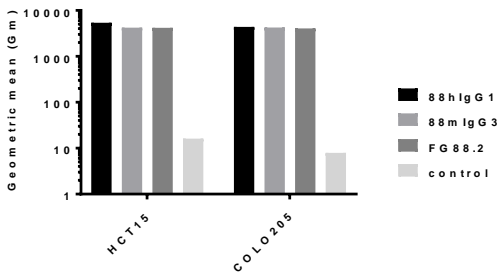
3 **Figure 6. i129G1, derived from a non-cytotoxic mlgG1 mAb, exhibits significant direct**
4 **cytotoxicity, enhanced avidity, pore forming ability as well as significant *in vivo* tumor control**
5 - Significantly increased proliferation inhibition (Panel A) and PI uptake (Panel B) on COLO205 (Panel
6 A) by i129G1 compared to 129hlgG1. Direct cell killing of low to moderate binding cancer cell lines
7 was negligible (Supplementary Fig. 3). Significantly increased functional affinity (SPR) by i129G1
8 compared to 129hlgG1 (Panel C). i129G1 maintains nanomolar ADCC activity on COLO205, but with
9 significantly reduced overall lysis compared to h129hlgG1 (Panel D). Nanomolar CDC activity by
10 i129G1 on COLO205 is significantly increased compared to 129hlgG1 (Panel E). Evidence of cellular
11 detachment, aggregation and pore forming ability by i129G1 on COLO205 using SEM, white arrows
12 point to irregular pores (Panel F). Significant *in vivo* tumor control by i129G1 compared to vehicle
13 control and compared to 129hlgG1 in a COLO205 xenograft model (Balb/c nude mice) (Panel G).
14 Individual tumor growth curves are shown in Supplementary Fig. 4. No significant effect on mean
15 body weight during the course of the mouse study (Panel H). Dose-dependent binding of rhFcRn by
16 i129G1 and 129hlgG1 at pH6.0 (Panel I). Significantly increased binding by i129G1 compared to
17 129hlgG1 at the top two concentrations. Negligible binding at pH7.0 by both constructs (Panel I).
18 Similar SEC-MALS profiles for i129G1 compared to 129hlgG1 (Panel J, i). A small increase in higher
19 MW species is evident in i129G1 compared to 129hlgG1 via AUC (Panel J, ii). No significant increase
20 in C4d generation upon incubation with human serum by i129G1, compared to 129hlgG1 (Panel J, iii).
21 Significance versus respective parental constructs was deduced from two-way ANOVA (direct
22 cytotoxicity, effector functions, rhFcRn binding, *in vivo* tumor control) or one-way ANOVA (functional
23 affinity and C4d detection), with Dunnett's corrections for multiple comparisons.

24

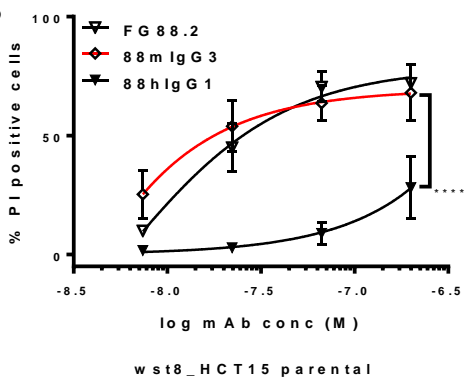
25

Figure 1

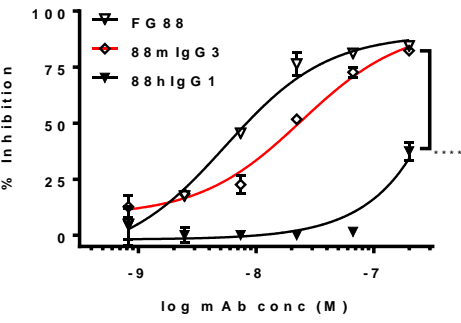
A



B



C



D

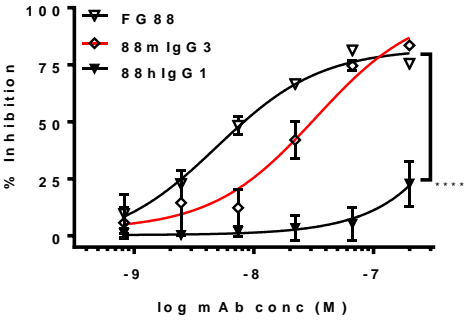


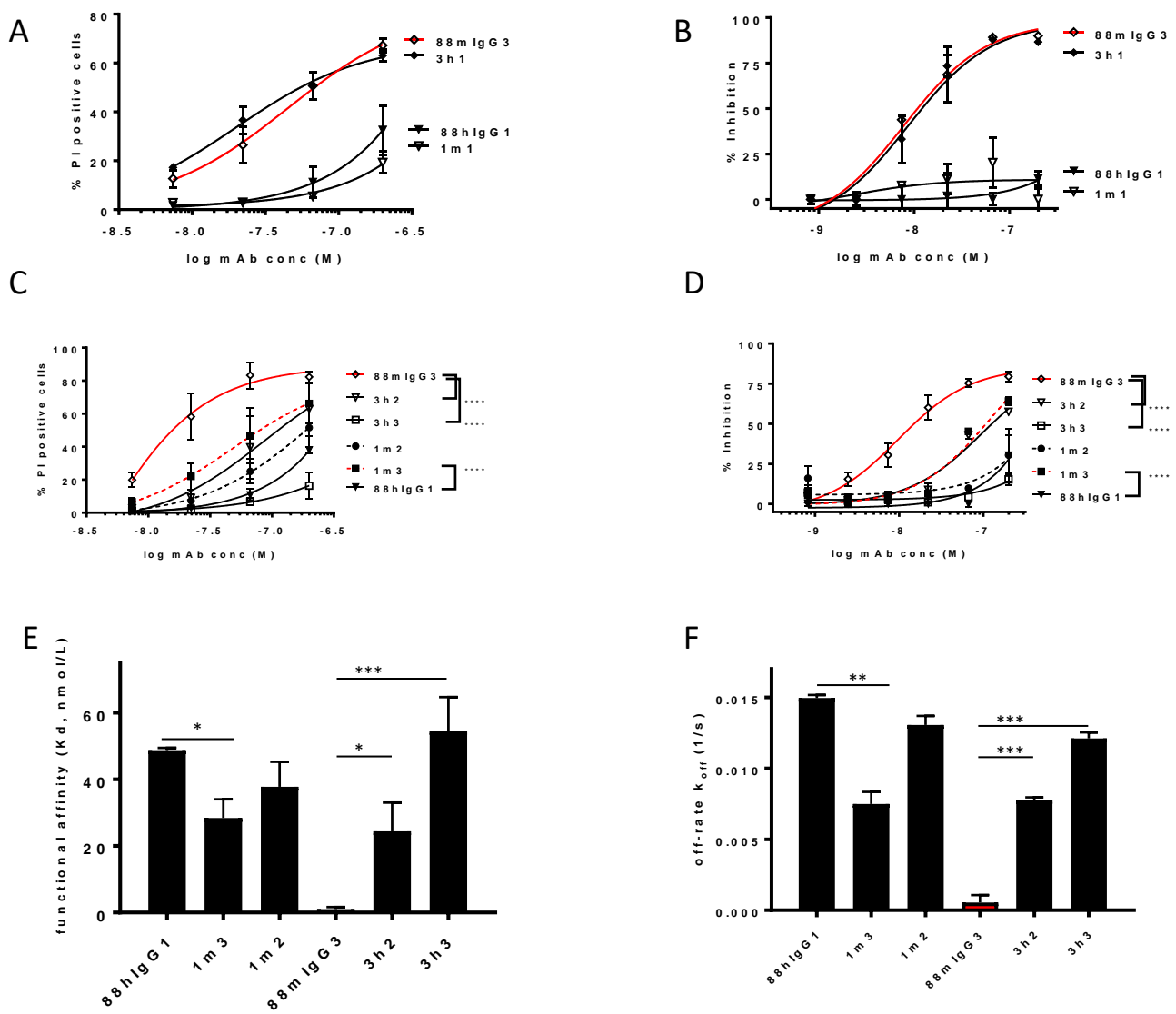
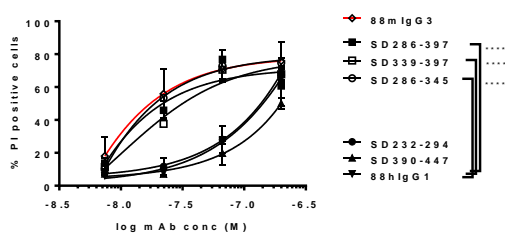
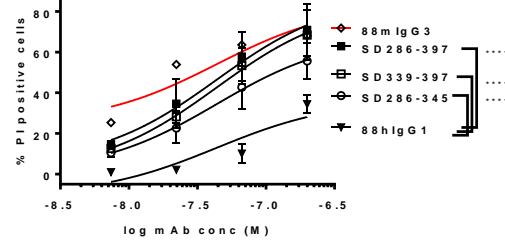
Figure 2

Figure 3

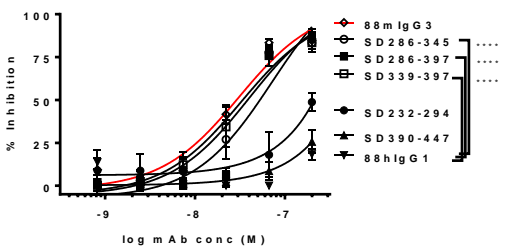
A



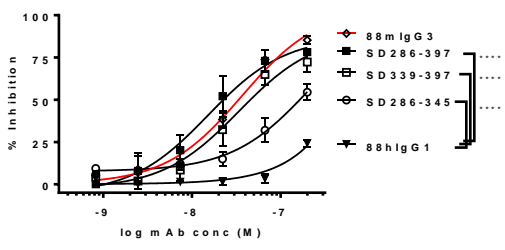
B



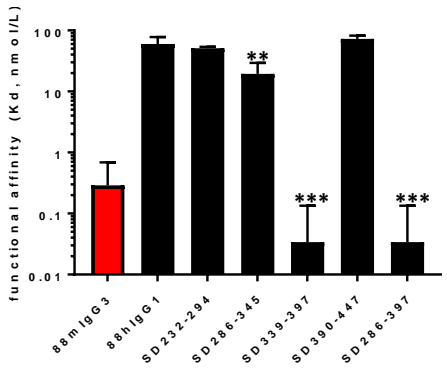
C



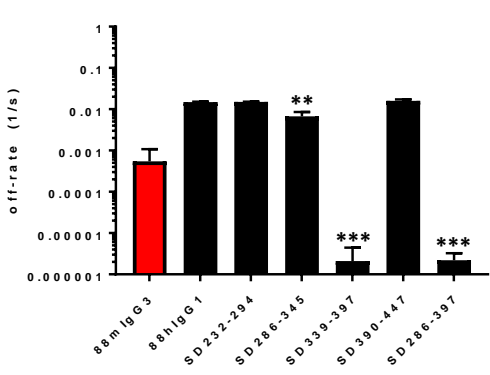
D



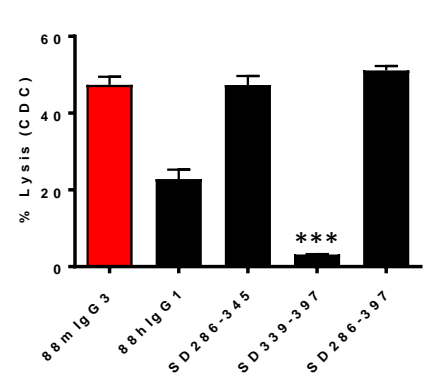
E



F



G



H

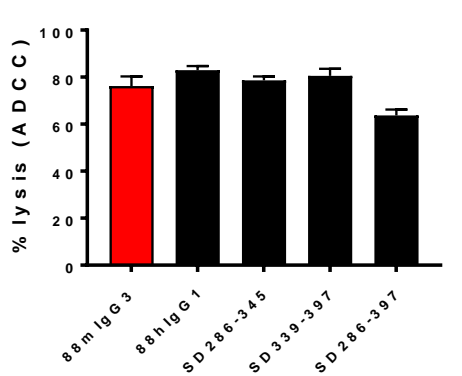


Figure 4

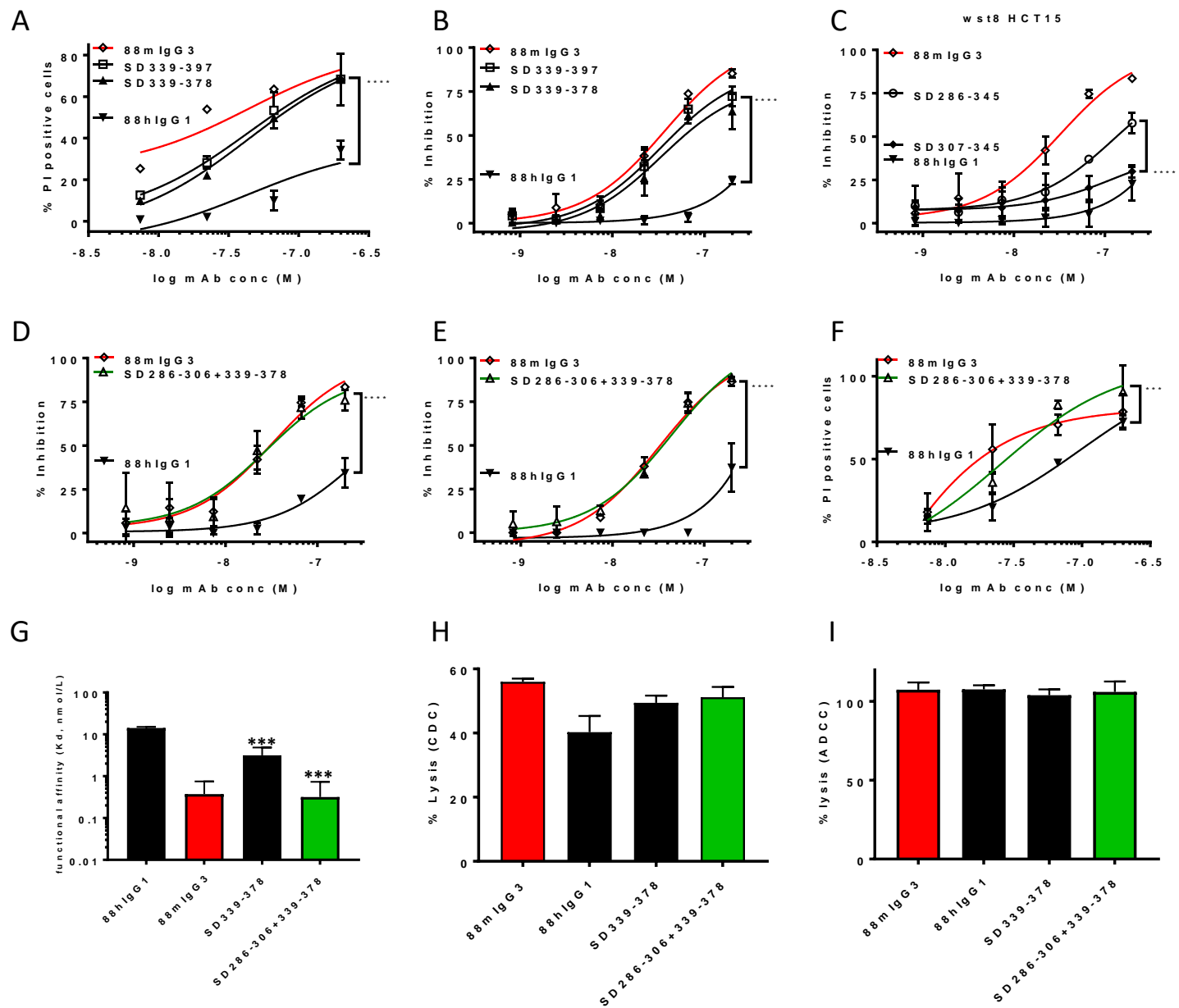
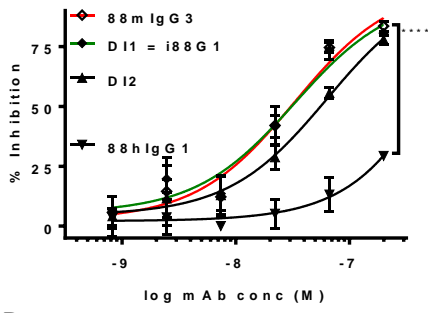
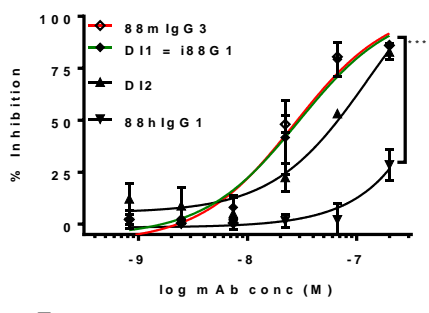


Figure 5

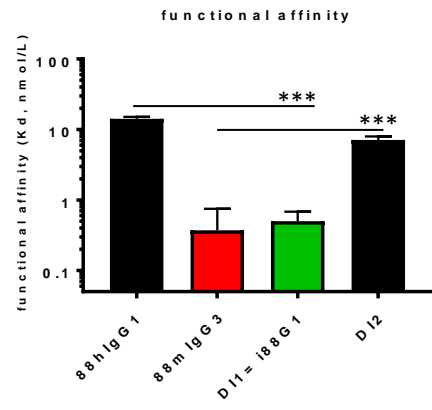
A



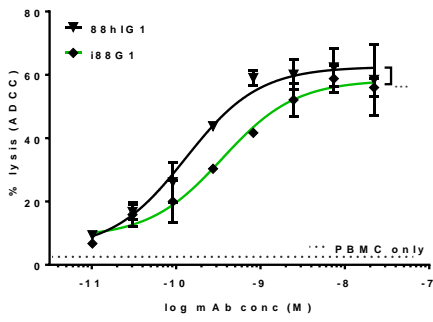
B



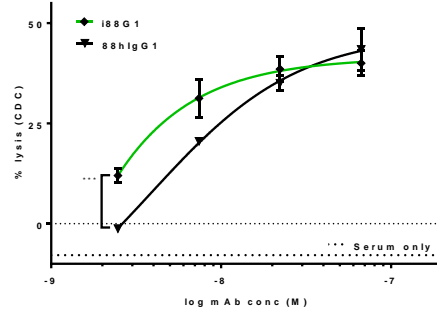
C



D



E



F

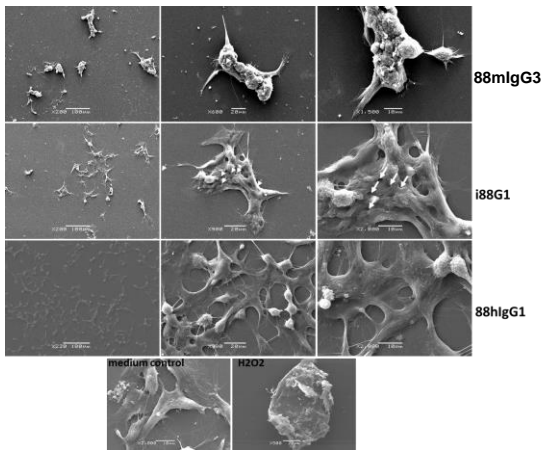


Figure 6